The Impact of Horizontal Resolution on the Tropical Heat Budget in an Atlantic Ocean Model

MARKUS JOCHUM

Massachusetts Institute of Technology, Cambridge, Massachusetts

RAGHU MURTUGUDDE

Earth System Science Interdisciplinary Center, College Park, Maryland

RAFFAELE FERRARI AND PAOLA MALANOTTE-RIZZOLI

Massachusetts Institute of Technology, Cambridge, Massachusetts

(Manuscript received 21 January 2004, in final form 6 July 2004)

ABSTRACT

An ocean general circulation model (OGCM) of the tropical Atlantic is coupled to an advective atmospheric boundary layer model. This configuration is used to investigate the hypothesis that resolving tropical instability waves (TIWs) in OGCMs will remove the equatorial cold bias that is a feature common to coarse-resolution OGCMs. It is shown that current eddy parameterizations cannot capture the TIW heat flux because diffusion in coarse-resolution OGCMs removes heat from the warm pool to heat the equatorial cold tongue, whereas TIWs draw their heat mostly from the atmosphere. Thus, they can bring more heat to the equatorial cold tongue without cooling the warm pool, and the SST in the warm pool is higher and more realistic. Contrary to expectations, the SST in the equatorial cold tongue is not significantly improved. The equatorial warming due to TIWs is slightly greater than the warming due to diffusion, but this increased equatorial heat flux in the high-resolution experiment is compensated by increased equatorial entrainment there. This is attributed to the Equatorial Undercurrent being stronger, thereby increasing the entrainment rate through shear instability. Thus, higher resolution does not significantly increase the total oceanic heat flux convergence in the equatorial mixed layer.

1. Introduction

SST is the principal ocean variable that affects the atmosphere. Prediction of the coupled ocean–atmosphere variability will always be limited by our ability to predict SST. To date, a rather impressive operational prediction of interannual variability of the coupled system has been achieved (Cane et al. 1986). However, shortcomings still remain (Davey et al. 2002). Especially in the Tropics the strong ocean–atmosphere feedback processes make it difficult to decide which model component is most in need of improvement: the ocean model, the atmosphere model, or the representation of air–sea interaction. The situation is further complicated by the large uncertainty of observed heat fluxes (Blumenthal and Cane 1989).

To understand the shortcomings of an ocean general circulation model (OGCM) in simulating SST one would ideally analyze an OGCM not coupled to an atmospheric general circulation model. However, it is common practice in uncoupled models to use boundary conditions that restore SST to climatological values or to use bulk parameterizations with specified air temperature and humidity; both choices mask potential errors in the oceanic mixed layer (ML) heat budget. Coupling the OGCM to an atmospheric boundary layer model (ABLM) such as that of Seager at al. (1995) removes these problems. Provided with observed wind velocity, SST, and incoming solar radiation the ABLM determines the atmospheric advection of heat and moisture and, thereby, the air–sea heat fluxes. Thus, the OGCM has much more freedom to develop its own SST and the SST reflects ocean physics rather than the constraints imposed by the boundary conditions.

Murtugudde et al. (1996) coupled this ABLM to the Gent and Cane (1989) OGCM and demonstrated that advection and diffusion of moisture play a significant role in determining the tropical SST in all three oceans.

Corresponding author address: Dr. Markus Jochum, Massachusetts Institute of Technology, 77 Massachusetts Avenue, 54-1410, Cambridge, MA 02139.
E-mail: markus@ocean.mit.edu

More importantly, at least in the context of the present study, the ABLM enabled them to determine that the main model flaw is the inadequate representation of the equatorial cold tongue (ECT) in the Atlantic and Pacific. Stockdale et al. (1993) also suggested that a too cold ECT is a critical factor in compromising the skill of OGCMs used in climate studies. Similarly, Davey et al. (2002) showed that the misrepresentation of the SST in the ECT is a general deficiency of OGCMs coupled to atmospheric models.

Since Hansen and Paul (1984), it is known that equatorial mesoscale eddies [commonly referred to as tropical instability waves (TIWs)] can make a significant contribution to the equatorial mixed layer heat budget. Based on the results of these observations and the coarse-resolution OGCM studies, we arrive at the following hypothesis: Resolving the TIWs in OGCMs will remove the cold bias of the ECT. For the present study it is assumed that the eddy-resolving OGCM realistically reproduces equatorial ocean dynamics and that shortcomings of the noneddy-resolving OGCM are due to an inadequate parameterization of subgrid-scale eddy processes. This study is focused on the Atlantic ocean but, since the phenomena dominating the heat budget (trade winds, ECT, and TIWs) are similar in the Pacific Ocean, the results of this study should apply there as well, at least qualitatively. Foltz et al. (2003) discuss the observed heat fluxes in the tropical Atlantic; however, the sharp equatorial gradients and high temporal variability in the ECT can only be resolved with an OGCM.

The next section describes the OGCM and the experiments, the third section discusses the equatorial heat budget in the different experiments, and the last section summarizes the results and their implications.

2. Model description

The OGCM employed for this study is the reduced gravity, primitive equation model of Gent and Cane (1989), which was specifically designed for studying the interactions between the dynamics and the thermodynamics of the upper tropical oceans. This model efficiently achieves fine vertical resolution below the mixed layer in regions of high vertical shear. The vertical structure of the model consists of a mixed layer above a fixed number of sigma layers.

The mixed layer depth and the thickness of the last sigma layer are computed prognostically and the remaining layers are computed diagnostically such that the ratio of each sigma layer to the total depth below the mixed layer is held to its prescribed value. The Lorenz N-cycle scheme (Lorenz 1971) is used for time integration and an eighth-order scale-selective Shapiro filter provides horizontal friction and diffusion. The lowest-order Shapiro filter is equivalent to Laplacian diffusion; higher orders are more scale selective (Gent and Cane 1989) but have the drawback that the contribution of diffusion to the heat budget cannot be easily recovered from the model results. To optimize the model solution, eighth-order filtering was chosen, and the diffusion of heat was estimated as the residual of the heat budget. The danger of this approach is that errors in the calculation could be misinterpreted as diffusion; however, the next section will show that the resulting diffusion in the high-resolution experiment is so small that we can be confident of our results.

A hybrid vertical mixing scheme was developed and embedded in the model by Chen et al. (1994). It combines the traditional bulk mixed layer model of the Kraus–Turner (1967) type with the dynamic instability model of Price et al. (1986) to simulate the three major processes of oceanic turbulent mixing: the bulk mixed layer model relates the atmospheric forcing to the mixed layer entrainment/detrainment; the gradient Richardson number mixing accounts for the shear flow instability; and an instantaneous adjustment simulates convection in the thermocline.

The OGCM is coupled to the ABLM that is described in Seager et al. (1995). Within this atmospheric mixed layer, the air temperature and air humidity are determined by a balance between surface fluxes, horizontal advection by prescribed winds, entrainment from above the mixed layer, and radiative cooling. This approach to determine the surface heat fluxes represents a clear improvement to the more traditional restoring boundary condition without the computational expense of a complete coupled model (Murtugudde et al. 1996).

For the present study, it must be emphasized that with an ABLM the OGCM has more liberty to seek its steady state than with traditional surface boundary conditions, that is, SST restoring or prescribed surface heat fluxes. The ABLM introduces nonlocal effects in the ocean heat budget through atmospheric advection of heat and moisture. This additional physics is essential to understand the model SST distribution. Through the ABLM each experiment computes its own latent and sensible heat flux, potentially creating large changes in the heat budget of models with identical boundary forcing.

In previous studies, this model has demonstrated its skill in reproducing the observed SST and circulation in the tropical Atlantic (Murtugudde et al. 1996; Inui et al. 2002) as well as the variability of the eddy field (Jochum et al. 2004b). The model is initialized with Levitus (1994) temperature and salinity fields, driven by monthly mean climatological Hellerman and Rosenstein (1983) winds, and its salinity and temperature are restored to Levitus (1994) in northern and southern sponge layers at 25°N and 25°S, respectively. Solar radiative forcing is taken from the Earth Radiation Budget Experiment (Li and Leighton 1993), cloud data is taken from Rossow and Schiffer (1991), and precipitation is based on Xie and Arkin (1998). Evaporation is

determined by the ABLM. The model has eight layers in the vertical for an average total depth of 600 m. Every simulation is spun up for 20 years, and the results discussed in the paper are taken from the subsequent 5 years of simulation. Two experiments are performed: a high-resolution experiment (H) with ¼° horizontal resolution and a low-resolution experiment (L) with 1 degree horizontal resolution. The model setups are identical otherwise. However, since the horizontal diffusion is determined by the Shapiro filter, which is of the same order in both runs, the effective horizontal diffusion is larger in L than in H because of the coarser resolution in L. A higher diffusivity in L could be interpreted as representing the effect of the eddies in H that are not resolved in L, but this is not the whole story, as will be discussed in the next section.

The annual mean SST and the variance of the meridional velocity on intra-annual time scales at the surface are shown for H in Fig. 1. In L, there is negligible eddy activity and the annual mean SST is lower everywhere (up to 1.5 K, see next section). While low eddy activity is to be expected in L, a lower SST is surprising and is explained in the next section. As motivated in the introduction, the present study will focus on the equatorial mixed layer and conclusions are restricted to this area only. Outside the deep Tropics the larger SST in H probably has different causes than the ones presented in the next section. For example, Nurser and Zhang (2000) and Oschlies (2002) discuss how baroclinic instability can raise the SST in midlatitudes.

3. The mixed layer heat budget

Jochum et al. (2004a, JMB hereafter) used a numerical model to show that the meridional eddy heat flux convergence due to TIWs (e.g., Hansen and Paul 1984) can partly be compensated by the associated vertical eddy heat flux. The equatorial mixed layer (ML), however, is so thin that even the residual eddy heat flux of approximately 30 W m^{-2} (in their model) is an important component of the heat budget. The hypothesis underlying the present study is that resolving the equatorial mesoscale eddy field (mainly TIWs, see Weisberg and Weingartner 1988; Foltz et al. 2004; JMB) will improve the representation of the ECT and remove the equatorial cold bias observed in the noneddy-resolving OGCM. Because of the complexity of the equatorial heat budget, simple physical reasoning provides little guidance for understanding the impact of TIWs on the equatorial SST. A more satisfactory approach is to compare the TIW-resolving experiment H with the noneddy-resolving experiment L.

The strip between 25° and 20°W is best suited for the analysis because it crosses the ECT and the warm pool to its north without intersecting land. These two areas are of central importance to the tropical Atlantic variability (Zebiak 1993; Chiang et al. 2002), and representing their SST correctly is the key to make progress in modeling tropical Atlantic variability. Increasing the resolution only marginally changes the mixed layer depth (Fig. 2) but significantly increases the SST and

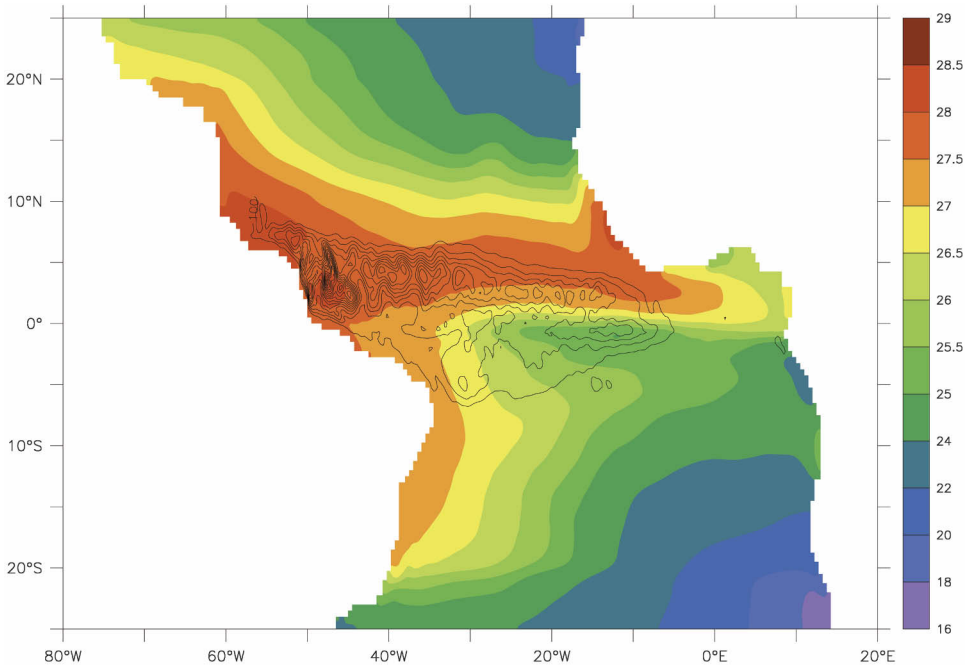

FIG. 1. Annual mean of the SST: superimposed is the variance of the meridional velocity in the mixed layer (contour lines: 100 cm^2 s^{-2}; the maximum is 1800 cm^2 s^{-2}). The seasonal cycle has been removed from the velocity before computing the variance.

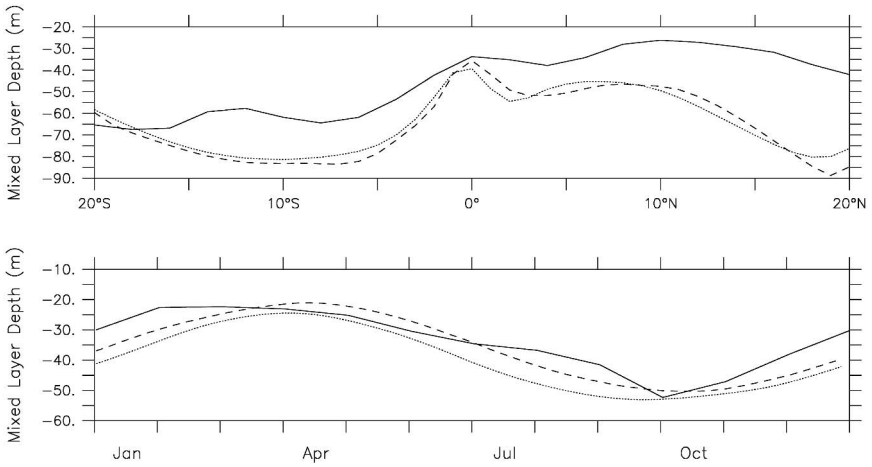

FIG. 2. Mixed layer depth averaged between 25° and 20°W for the observations (from de Boyer Montegut et al. 2004) (solid line), H (dashed line), and L (dotted line): (top) a longitudinal section of the annual mean and (bottom) the seasonal cycle at the equator. Note that in the model the ML depth is a prognostic variable whereas in the observations it cannot be defined based on first principles. Especially in areas of weak stratification, the ML depth can vary significantly for slightly different definitions.

the equatorward SST gradient (Fig. 3). Comparison with the observations leads to the conclusion that the overall SST is improved but that the cold tongue is still too cold. Also, the SST difference between the warm pool and the cold tongue in H is larger than in the observations of any single year (not shown). Contrary to expectations, increasing the resolution leads to an improvement of the SST in the warm pool and not in the cold tongue. The following analysis of the heat budget will explain this result and lead to new insights in the role of TIWs in the equatorial heat budget.

The heat budget for the ML is (Stevenson and Niiler 1983) given by

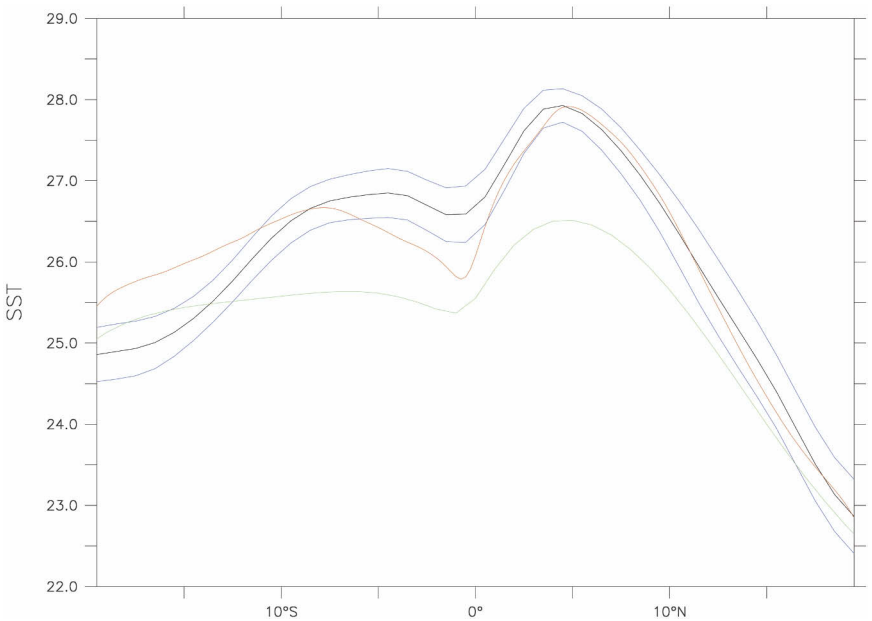

FIG. 3. Annual mean SST averaged between 25° and 20°W for Reynolds and Smith (1994); (black line: mean; blue lines: ±1 standard deviation), H (red line), and L (green line). The close similarity in SST between the observations and H north of 2°N is not the result of any parameter tuning but should not be taken as an indication of a perfect model either. The important point is that SST in H is increased *and* improved.

$$c_p\rho h(T_t + \mathbf{v}\cdot\boldsymbol{\nabla}\mathbf{T}) = Q_{\text{atmos}} - Q_{\text{ent}} + Q_{\text{diff}}. \quad (1)$$

Here $\mathbf{T}$ is the SST, ρ is the density, and c_p is the heat capacity of seawater, h is the ML depth, $\mathbf{v}$ is the horizontal velocity vector, Q_{atmos} is the net surface heat flux from the atmosphere, Q_{ent} is the cooling of the ML due to entrainment of water from below, and Q_{diff} is the horizontal diffusion of heat in the OGCM, intended to represent unresolved eddy transports. Dividing by $c_p\rho h$ and averaging over the 5 yr of model output yields

$$\overline{\mathbf{v}_s\cdot\boldsymbol{\nabla}T_s} + \overline{\mathbf{v}_s\cdot\boldsymbol{\nabla}T'} + \overline{\mathbf{v}'\cdot\boldsymbol{\nabla}T_s} + \overline{\mathbf{v}'\cdot\boldsymbol{\nabla}T'} = \overline{q_{\text{atmos}}} - \overline{q_{\text{ent}}} + \overline{q_{\text{diff}}}, \quad (2)$$

where the overbar denotes the 5 yr mean; the SST and the velocities have been split into mean plus seasonal cycle (subscript s) and eddy component (superscript prime). The mean plus seasonal cycle has been determined by averaging over the monthly values of all years, and the eddy components are the deviations from these mean plus seasonal values. The first term on the lhs is the contribution of the mean and the seasonal cycle to the heat budget, and the next three terms are the eddy contributions (since they would be zero without eddies; see Kessler et al. 1998). The reason for this somewhat unusual split is that it facilitates the comparison between L, which can be expected to reproduce the seasonal cycle but not the eddy fluxes, and H, which resolves both. The components of the budget in (2) can be computed from the model output to estimate what processes determine the SST.

The heat budget for H (Fig. 4) is similar to the one obtained by JMB, who studied an eddy-resolving level model [the Princeton Modular Ocean Model (MOM2b)] driven by the same winds as H, but with SST restoring as boundary conditions and the Pacanowski and Philander (1981) vertical mixing scheme. The main difference is that the TIW contribution to the ML heat budget in JMB is 50% smaller than in H and the mean advection of heat in H is 50% smaller than in JMB. The contribution of entrainment and atmospheric net heat flux are approximately equal. Given the very different vertical mixing parameterization and thermal boundary conditions in the two experiments, this is a reassuring result. However, one of the motivations of the present study is that in JMB the ML is not properly resolved and the SST restoring introduces spurious heat sources. These shortcomings are overcome in the present study through the addition of an ABLM and a more realistic ocean ML model.

The similarity of the mean and seasonal advection of heat (red line in Figs. 4 and 5) in H and L demonstrates that the seasonal signal is well resolved in L and that the scale separation between the seasonal and high frequency signals is large enough to justify the split in Eq. (2). North of the equator the mean and seasonal heat advection is dominated by the meridional component that moves upwelled cold water poleward through Ekman dynamics, whereas south of the equator zonal and

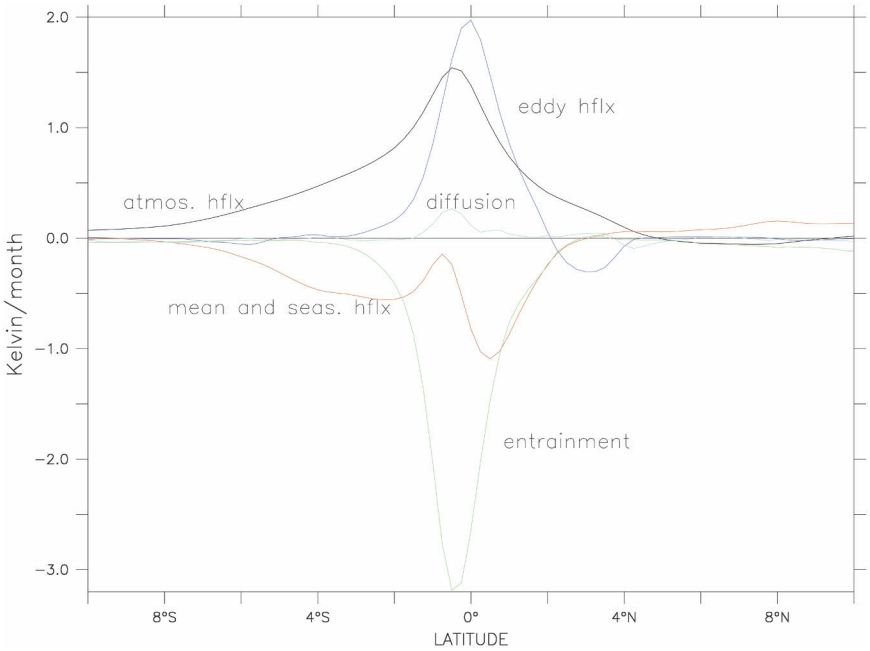

FIG. 4. Annual mean heat budget for H averaged between 25° and 20°W. Black: net surface heat flux, the red line is the mean and seasonal advection of heat, the dark blue line is eddy heat fluxes, light blue: horizontal diffusion, and green line: entrainment and vertical diffusion. Units are kelvin month^{-1}.

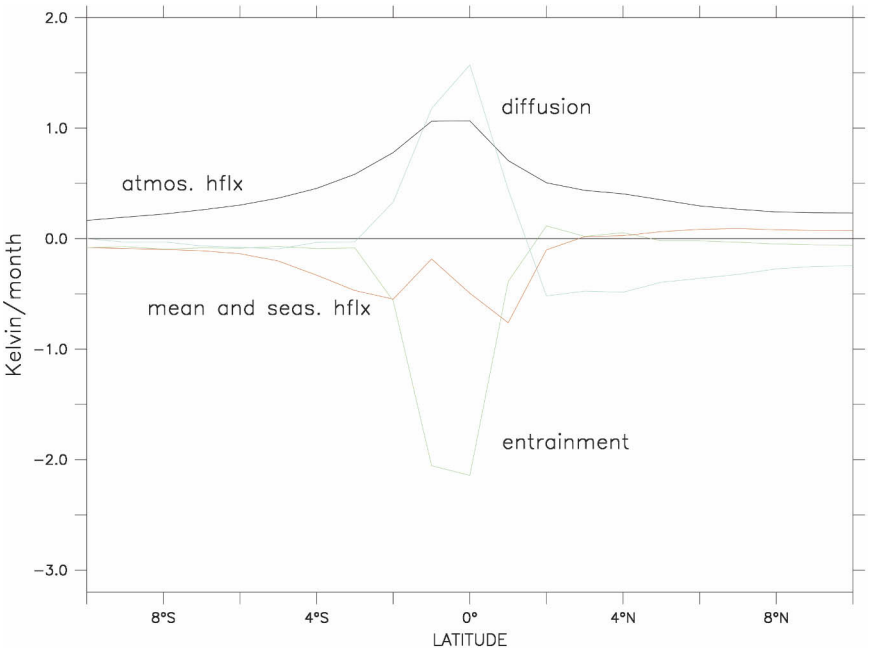

FIG. 5. As in Fig. 4 but for L. Eddy heat fluxes are negligible.

meridional advection are approximately of equal importance. On and near the equator (1°S–1°N), zonal advection dominates, which is in accordance with the observations by Foltz et al. (2003).

Comparing Figs. 4 and 5 shows that the lower SST in the warm pool of L is caused by horizontal diffusion (light blue line), which is almost absent in H. It moves heat away from the warm pool toward higher latitudes and the equator. This happens, but to a lesser degree, south of the equator as well. The horizontal diffusion in L, which supposedly represents the mixing of the unresolved mesoscale eddy field, overestimates the lateral mixing by eddies away from the equator. However, between 2°S and 2°N the Shapiro filter (Fig. 5, light blue) performs surprisingly well and reproduces approximately 85% of the eddy heat flux convergence (Fig. 4, dark blue). Thus, while in the ocean interior the eddies seem to move heat around adiabatically (Gill et al. 1973; Gent and McWilliams 1990), they can lead to diabatic heating in the ML, which suggests that there they can be represented by simple horizontal diffusion. The fact that eddies act differently in the interior and the surface is not captured well in current eddy parameterizations (Ferrari and McWilliams 2004, manuscript submitted to *Ocean Modell.*).

It should be noted that in L, in contrast to H, the heating of the ECT comes at the expense of the warm pool. This is a major result of the present study. In H, the area from 4°S to 2°N is heated with 2.4×10^7 W m^{-1}, whereas the area from 2°N to 4°N is only cooled at a rate of 0.4×10^7 W m^{-1}. This supports the dynamical analysis of JMB, who show that the TIWs are caused by barotropic rather than baroclinic instability. Baroclinic instability implies an adiabatic flattening of isotherms in which water from the warm pool is moved on top of the ECT water. In H, little warm pool heat is lost due to the TIWs (this also indicates that the breaking of TIW crests is only of minor importance). Rather, the TIWs advect cold water poleward where it experiences a strong atmospheric heat flux and return it half a wave period later as warm water. A simple calculation can illustrate the power of this heat engine: the typical ML depth is 30 m, the average atmospheric heat flux is 100 W m^{-2}, and the TIW wave period is about 30 days. In the absence of other processes, a water parcel would return to the ECT 1 K warmer, which yields the 2°C $month^{-1}$ heating rate of the TIWs in H (Fig. 4). Of course, the heat gain would be the same if the parcel does not move, but *only* if the entrainment cooling was switched off. Thus, the key to explain the strong heating of the TIWs is that they move water away from the equatorial cooling, let it heat up by the atmosphere, and then return it. At the equator the heat is then entrained into the thermocline by the strong vertical mixing. Thus, TIWs do not advect heat away from the tropical warm pool; rather, they act, together with the strong vertical mixing at the equator, as a vertical heat pump that takes heat from the atmosphere and puts it into the thermocline. This result is not unique to the present model or the Atlantic TIWs. Revisiting earlier studies shows that this also happens in z-level models with SST restoring (JMB) or in the equatorial Pacific (Kessler et al. 1998).

The above description of the mechanism by which TIWs transport heat is extremely simplified. It is highlighted here because it represents a paradigm shift in

the way to think about TIW heat fluxes—one must abandon simple mixing length arguments and talk in terms of nonlocal effects of entrainment and atmospheric heat flux. Of course, TIW heat flux convergence includes additional components due to wave breaking (e.g., Kessler et al. 1998), and zonal (e.g., Weingartner and Weisberg 1991) and vertical (JMB) wave fluxes, none of which are necessarily negligible. In a preliminary study, we find that the split between meridional and zonal heat fluxes may be different in the Pacific and Atlantic Oceans. However, a detailed discussion of these different contributions is beyond the scope of the present hypothesis and will be published in a separate study.

Another important result is that the entrainment cooling (green line) in L is *less* than in H (by approximately 20% when averaged between 2°S and 2°N). Thus, higher horizontal resolution leads to an increased downward diffusion of heat. The model's ML computes the entrainment from buoyancy forcing, wind stirring, and vertical shear instability. The wind stress is the same in both experiments and the buoyancy forcing is very similar (see details later in the text). Thus, the difference must come from stronger shears below the ML. The entrainment cooling is largest near the equator because strong Ekman suction leads to a minimum in ML depth. There, the onset of the strong cooling in early spring coincides with a threefold increase of the equatorial wind stress from April to July (Fig. 6). In contrast to L, the cooling in H continues to strengthen after June and is larger than in L until late fall when the winds weaken in response to the approaching ITCZ. In L, the maximum cooling is reached in June, whereas in H the cooling is largest in July (Fig. 6). The ML depth and stratification are only marginally different between H and L; therefore the larger entrainment in H must be due to larger vertical shears in velocity that are significantly larger in H than in L (Fig. 7).

A comparison of Q_{ent} in H and L (Fig. 6) suggests

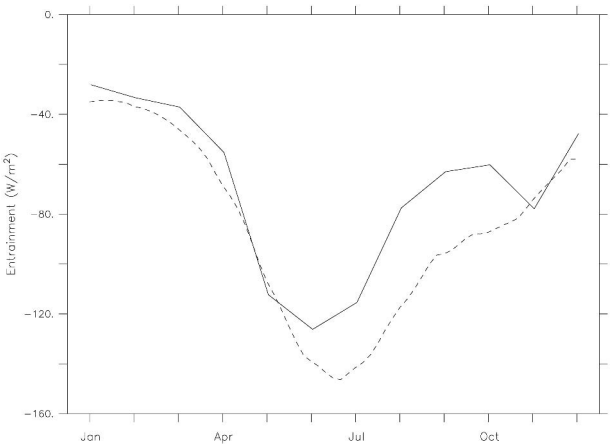

FIG. 6. The annual cycle of entrainment on the equator averaged between 25° and 20°W. Solid line: L; broken line: H.

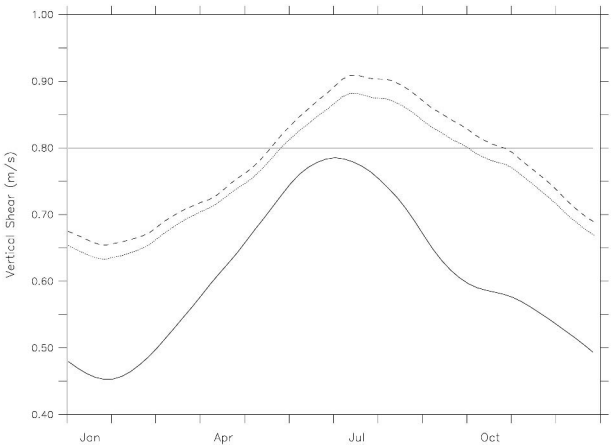

FIG. 7. The seasonal cycle of the velocity difference on the equator between the SEC and EUC for L (solid line), H (dashed line), and H with TIWs filtered out (dotted line).

that the shear only contributes to enhanced entrainment from May to November, which matches the time when the velocity difference between ML and the Equatorial Undercurrent (EUC) in H exceeds 0.8 m s^{-1} [Fig. 7, for a review of EUC dynamics see Pedlosky (1996)]. Such a large threshold is consistent with the findings of Chen et al. (1994) that adding shear instability to the Krauss–Turner (1967) mixing scheme of their *coarse*-resolution model does not change the SST significantly. The empirical threshold of a velocity difference of 0.8 m s^{-1} between EUC and ML suggests a critical bulk Richardson number of approximately 0.7. This is close to 0.65, the threshold value that leads to instant vertical mixing in the mixing scheme of Price et al. (1986). Unlike the gradient Richardson number (Ri), which is based on shears between two adjacent layers, the bulk Richardson number is based on shears over a larger vertical extent, in this case the shear between ML and EUC core. The model employs a critical Ri of 0.25, which should have been sufficient to analyze the entrainment. However, we find that evaluating Ri from the model output is not helpful in analyzing the results because the model fields are saved *after* the mixing has taken place. Furthermore, the shear-driven mixing may successively involve all layers from the surface down to the EUC, making it difficult to use Ri criteria locally.

It is not obvious whether the increased shear that leads to the larger entrainment in H is due to faster mean currents or TIWs, which are absent in L but of realistic strength in H (Jochum et al. 2004b). Distinguishing between these two effects is difficult because the TIWs are generated by barotropic instability of the EUC (JMB). Thus, the seasonal cycle of the EUC leads to a seasonal cycle of the TIW-induced mixing, which obstructs its quantification. An estimate of mean versus TIW-induced shear can be obtained as follows: the equatorial currents maintain their structure over the

distance of one TIW wavelength (800–1000 km); therefore averaging the velocity field from 26° to 18°W filters out most of the shear due to TIWs but retains shear due to mean currents (time averaging over the average TIW period leads to similar results). Hence, we will compare

$$\langle[(u_{\text{surface}} - u_{\text{EUC}})^2 + (v_{\text{surface}} - v_{\text{EUC}})^2]^{1/2}\rangle$$

with

$$[(\langle u_{\text{surface}}\rangle - \langle u_{\text{EUC}}\rangle)^2 + (\langle v_{\text{surface}}\rangle - \langle v_{\text{EUC}}\rangle)^2]^{1/2},$$

where angle brackets denotes an average from 26° to 18°W. The first measure of shear retains the component due to TIWs whereas the second one averages over one wavelength, thereby filtering out the impact of TIWs on shear. The difference between the two measures of vertical shear is rather small (Fig. 7), suggesting that TIW-induced shear makes only a small contribution to the vertical shear (this is true for the shear between any other two layers as well). Thus, the difference in entrainment between H and L is mostly due to an increased mean current strength. The South Equatorial Current (SEC) at the surface is directly driven by the wind and is not significantly different in H and L, but the EUC velocities are approximately 30% weaker in L compared to H, making the faster EUC the main reason for the stronger entrainment there.

A surprising result of the present comparison is that the atmospheric heat flux into the ECT is larger in H than L—by 15% when averaged from 2°S to 2°N—although the SST is larger in H than in L (Figs. 3, 4, and 5). Since the incoming solar radiation is identical in both cases and the outgoing longwave radiation increases with SST, the difference must be due to differences in the sensible and latent heat fluxes. The total annual difference in heat flux is 14 W m^{-2}, 30% of which is contributed by sensible heat flux and 70% by latent heat flux (Fig. 8). In standard heat flux parameterization schemes both sensible and latent heat loss would be larger in H because of the larger SST. In the present study, the ABLM advection of heat and moisture can change this simple local balance (Murtugudde et al. 1996). Indeed we find that warm and moist air is advected from south of the equator over the ECT by the southeast trades. Because the SST gradients are much sharper in H than in L (Figs. 3 and 9), the ocean warming is larger in H. This effect is particularly strong in July when the trades and the ECT are so strong that the sensible heat flux in H can *heat* the ML (Fig. 8).

4. Summary and discussion

Based on literature of tropical ocean modeling and TIWs, we were led to the hypothesis that resolving TIWs in OGCMs will remove the cold bias of the ECT in coarse-resolution OGCMs. This hypothesis was rejected with the analysis given in the present paper, and new insights were gained into details of the equatorial ML heat budget and are reported here. The most important result is that TIWs *do not heat* the ECT with heat advected from the warm pool. Instead, they draw their heat from the atmosphere. In L, the diffusion that represents the TIWs heats the ECT by drawing heat from the warm pool, decreasing the SST there. With the ABLM we quantified this effect; spurious diffusion leads to approximately 1-K cooler extraequatorial Tropics. In H, the TIW move water away from the equatorial regions of strong entrainment cooling, let it heat up by the atmosphere, and then return this warmer water. The heat is drawn from the atmosphere and it is not necessary to exchange water with the warm pool.

Secondly, better resolution leads to stronger vertical mixing and stronger cooling in the ECT, which offsets the increased warming due to the TIWs. This is due to a stronger EUC and the increased mixing due to larger

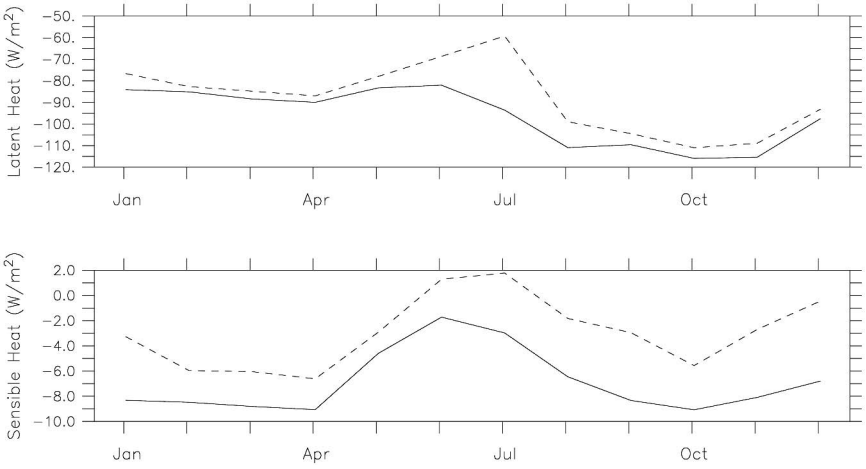

FIG. 8. The seasonal cycle of the (top) latent and (bottom) sensible heat flux at the equator between 25° and 20°W for H (dashed line) and L (solid line). Note the difference in scale.

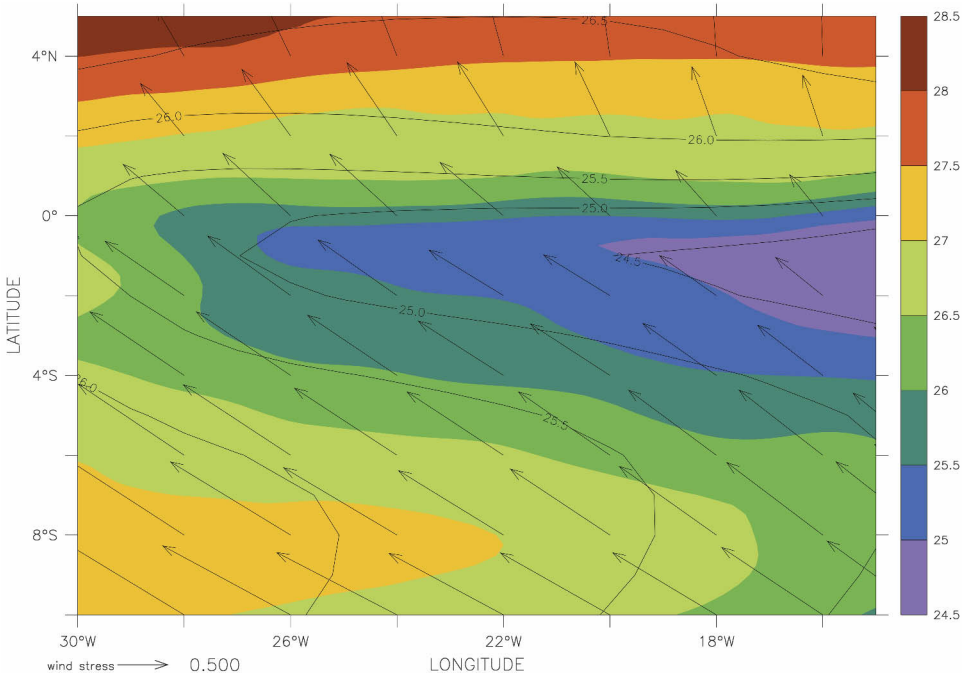

FIG. 9. The July SST in the central Tropics for H (colored) and L (contour lines every 0.5 K). Overlaid is the Jul wind stress. Note how the southeast trades blow from warm water to the cold water in the ECT in both experiments but cross more isotherms in H.

vertical velocity shears. This implies that, although the total oceanic heat flux convergence is similar in H and L, more heat is pumped into the equatorial thermocline, leading to a 20% weaker stratification in the upper 100 m (not shown).

A third difference between H and L is found in the sensible and latent heat fluxes. The southeast trades advect moist and warm air across the ECT, which reduces the latent and sensible heat flux there. Although the ECT is warmer in H, this effect is larger there because of the sharper SST gradient. Notice, though, that the meridional SST gradient is more realistic in L than in H (Fig. 3), suggesting that atmospheric advection of heat and moisture is exaggerated in H. The caveat is that, in reality, the winds would respond to a changed SST. Therefore, this particular result is likely a numerical artifact, which emphasizes the importance of using a *dynamic atmosphere* in studies of the upper ocean.

Clearly, higher resolution does not remove or improve the cold bias of the ECT in this numerical model. Since the reason for this is the increased shear instability of the EUC whose effect is parameterized, this particular result may differ from model to model. However, independent of the model is the finding that in coarse-resolution models TIWs cannot be represented by lateral diffusion. Rather than moving heat laterally from the warm pool to the cold tongue, TIWs carry heat that is drawn from the atmosphere toward the equator over the highly sheared EUC, where the heat is mixed downward. This requires a new parameterization that will be the focus of the authors' future work.

The original hypothesis to explain the cold tongue bias in terms of TIW heat advection was rejected; therefore, a crucial component of the ECT heat budget is still missing. It is not clear whether the missing component produces simply an offset or contributes to the seasonal cycle as well. Comparison of the seasonal cycles of SST in H, L, and observations shows that not only is the mean SST too cold in the model ECT, but also that the SST seasonal cycle is too weak. Moreover, the bias does not depend on resolution (Fig. 10). The model produces not enough warming during fall and not enough cooling

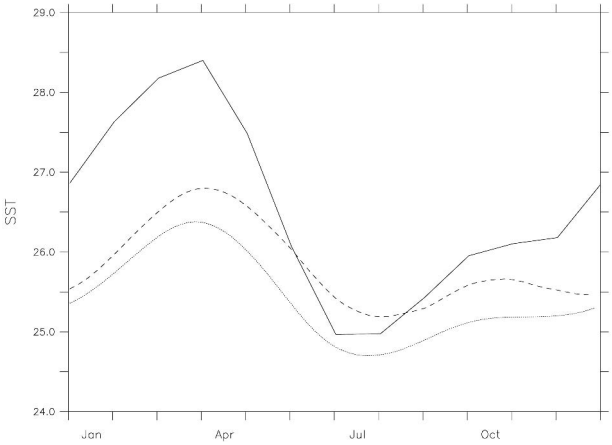

FIG. 10. Seasonal cycle of SST averaged between 25° and 20°W and between 1°S and the equator for Reynolds and Smith (1994) (solid line), H (dashed line), and L (dotted line).

during spring. These differences could be removed by adding a correction of less than 20 W m^{-2} during fall (about the uncertainty of the observed ocean–atmosphere heat flux) and removing it during spring, but it is difficult to justify these corrections on physical grounds. Most certainly, the amplitude problem rules out a systematic error in the solar radiation data. Similarly, uniformly changing the drag coefficient that converts wind speed into wind stress, or the bouyancy and wind-stirring coefficients that determine the ML depth, is unlikely to improve the solution over all. It may improve the SST during one season but only at the expense of a worse performance during other seasons. This was seen already for the annual mean SST by Murtugudde et al. (1996); changing the above parameters to improve the SST in the ECT worsens the SST elsewhere.

There is a long list of physical processes that could improve the seasonal cycle along the equator but they have been omitted in the present model configuration. For example, seasonal variations in high-frequency wind forcing or the diurnal cycle in the buoyancy forcing could be relevant. Since the thermodynamics of the ML is nonlinear, these processes could make an important contribution to the heat budget. Hashizume et al. (2001) and Chelton et al. (2001) both observe strong coupling between the TIW-induced SST anomalies and the local wind stress. These effects can possibly be parameterized and included into the ABLM to study whether this local coupling makes a net contribution to the ML heat budget. Another interesting process is discussed by Murtugudde et al. (2002), who find that the oceanic chlorophyll distribution leads to spatial variations in the attenuation depth of solar radiation. Finding a sound physical representation for all these different processes is not trivial, and we choose to focus on the effect of TIWs in this paper.

Acknowledgments. The authors thank Gregory Foltz, Antonio J. Busalacchi, and one anonymous reviewer for helpful suggestions. This research was funded with NOAA Grant NA16GP1576 and NASA Grant NAG5-7194 at MIT.

REFERENCES

Blumenthal, M., and M. Cane, 1989: Accounting for parameter uncertainties in model verification: An illustration with tropical SST. *J. Phys. Oceanogr.,* **19,** 815–830.

Cane, M., S. Dolan, and S. Zebiak, 1986: Experimental forecasts of the 1982/83 El Niño. *Nature,* **321,** 827–832.

Chelton, D. B., and Coauthors, 2001: Observations of coupling between surface wind stress and sea surface temperature in the eastern tropical Pacific. *J. Climate,* **14,** 1479–1498.

Chen, D., L. Rothstein, and A. Busalacchi, 1994: A hybrid vertical mixing scheme and its applications to tropical ocean models. *J. Phys. Oceanogr.,* **24,** 2156–2179.

Chiang, J., Y. Kushnir, and A. Giannini, 2002: Deconstructing Atlantic Intertropical Convergence Zone variability: Influence of the local cross-equatorial sea surface temperature gradient and remote forcing from the eastern equatorial Pacific. *J. Geophys. Res.,* **107**, 4004, doi:10.1029/2000JD000307.

Davey, M., and Coauthors, 2002: STOIC: A study of coupled model climatology and variability in tropical ocean regions. *Climate Dyn.*, **18**, doi:10.1007/s00382–001–0188–6.

de Boyer Montegut, C., A. Fischer, A. Lazar, D. Iuducone, and G. Madec, 2004: A global mixed layer depth based on individual profiles. *J. Geophys. Res.,* in press.

Foltz, G., S. Grodsky, J. Carton, and M. McPhaden, 2003: Seasonal mixed layer heat budget of the tropical Atlantic Ocean. *J. Geophys. Res.*, **108**, 3146, doi:10.1029/2002JC001584.

——, J. Carton, and E. Chassignet, 2004: Tropical instability vortices in the Atlantic Ocean. *J. Geophys. Res.,* **109,** C03029, doi:10.1029/2003JC001942.

Gent, P., and M. Cane, 1989: A reduced gravity, primitive equation model of the upper equatorial ocean. *J. Comput. Phys.,* **81,** 444–480.

——, and J. McWilliams, 1990: Isopycnal mixing in ocean circulation models. *J. Phys. Oceanogr.,* **20,** 150–155.

Gill, A., J. Green, and A. Simmons, 1973: Energy partition in the large-scale circulation and the production of mid-ocean eddies. *Deep-Sea Res.,* **21,** 499–527.

Hansen, D., and C. Paul, 1984: Genesis and effects of long waves in the equatorial Pacific. *J. Geophys. Res.,* **89,** 10 431–10 440.

Hashizume, H., S. Xie, T. Liu, and K. Takeuchi, 2001: Local and remote atmospheric response due to tropical instability waves: A global view from space. *J. Geophys. Res.,* **106,** 10 173–10 185.

Hellerman, S., and M. Rosenstein, 1983: Normal monthly wind stress over the world ocean with error estimates. *J. Phys. Oceanogr.,* **13,** 1093–1104.

Inui, T., A. Lazar, P. Malanotte-Rizzoli, and A. Busalacchi, 2002: Wind stress effects on subsurface pathways from the subtropical to tropical Atlantic. *J. Phys. Oceanogr.,* **32,** 2257–2276.

Jochum, M., P. Malanotte-Rizzoli, and A. Busalacchi, 2004a: Tropical instability waves in the Atlantic Ocean. *Ocean Modell.,* **7,** 145–163.

——, R. Murtugudde, P. Malanotte-Rizzoli, and A. Busalacchi, 2004b: Internal variability in the Atlantic Ocean. *Earth's Climate: The Ocean–Atmosphere Interaction*, *Geophys. Monogr.*, No. 147, Amer. Geophys. Union, 181–187.

Kessler, W. S., L. M. Rothstein, and D. Chen, 1998: The annual cycle of SST in the eastern tropical Pacific as diagnosed in an OGCM. *J. Climate,* **11,** 777–799.

Kraus, E., and J. Turner, 1967: A one-dimensional model of the seasonal thermocline. Part II. *Tellus,* **19,** 98–105.

Levitus, S., 1994: *Climatological Atlas of the World Ocean*. NOAA Prof. Paper 13, 173 pp. and 17 microfiche.

Li, Z., and H. Leighton, 1993: Global climatologies of the solar radiation budgets form 5 years of ERBE data. *J. Geophys. Res.,* **98,** 4919–4930.

Lorenz, E., 1971: An *N*-cycle time-differencing scheme for stepwise numerical integration. *Mon. Wea. Rev.,* **99,** 644–648.

Murtugudde, R., R. Seager, and A. Busalacchi, 1996: Simulation of the tropical oceans with an ocean GCM coupled to an atmospheric mixed layer model. *J. Climate,* **9,** 1796–1815.

——, J. Beauchamp, C. McClain, M. Lewis, and A. Busalacchi, 2002: Effects of penetrative radiation on the upper tropical ocean circulation. *J. Climate,* **15,** 470–486.

Nurser, A., and J. Zhang, 2000: Eddy-induced mixed layer shallowing and mixed layer/thermocline exchange. *J. Geophys. Res.,* **105,** 21 851–21 868.

Oschlies, A., 2002: Improved representation of upper-ocean dynamics and mixed layer depths in a model of the North Atlantic on switching from eddy-permitting to eddy-resolving grid resolution. *J. Phys. Oceanogr.,* **32,** 2277–2298.

Pacanowski, R., and S. Philander, 1981: Parameterization of vertical mixing in numerical models of the oceans. *J. Phys. Oceanogr.,* **11,** 1443–1451.

Pedlosky, J., 1996: *Ocean Circulation Theory*. Springer, 453 pp.

Price, J., R. Weller, and R. Pinkel, 1986: Diurnal cycle: Observations and models of the upper ocean response to diurnal heating, cooling and wind mixing. *J. Geophys. Res.,* **91,** 8411–8427.

Reynolds, R., and T. Smith, 1994: Improved global SST analyses using optimal interpolation. *J. Climate,* **7,** 929–948.

Rossow, W. B., and R. A. Schiffer, 1991: ISCCP cloud data products. *Bull. Amer. Meteor. Soc.,* **72,** 2–20.

Seager, R., M. Blumenthal, and Y. Kushnir, 1995: An advective atmospheric mixed layer model for ocean modeling purposes: Global simulation of atmospheric heat fluxes. *J. Climate,* **8,** 1951–1964.

Stevenson, J., and P. Niiler, 1983: Upper ocean heat budget during the Hawaii-to-Tahiti Shuttle Experiment. *J. Phys. Oceanogr.,* **13,** 1894–1907.

Stockdale, T., and Coauthors, 1993: Intercomparison of tropical ocean GCMs. World Circulation Programme Research Memo. WCRP-79, 67 pp.

Weingartner, T., and R. Weisberg, 1991: A description of the annual cycle in sea surface temperature and upper ocean heat in the equatorial Atlantic. *J. Phys. Oceanogr.,* **21,** 83–96.

Weisberg, R., and T. Weingartner, 1988: Instability waves in the equatorial Atlantic Ocean. *J. Phys. Oceanogr.,* **18,** 1641–1657.

Xie, P. P., and P. A. Arkin, 1998: Global monthly precipitation estimates from satellite-observed outgoing longwave radiation. *J. Climate,* **11,** 137–164.

Zebiak, S., 1993: Air–sea interaction in the tropical Atlantic. *J. Climate,* **6,** 1567–1586.